Passive discrete lens for broadband elastic guided wave focusing

Emeline Sadoulet-Reboul, Gaël Matten, Kaijun Yi, Morvan Ouisse

OVERLAY

Journal of Theoretical, Computational and Applied Mechanics

JTCAM

DIAMOND OPEN ACCESS

Identifiers
DOI 10.46298/jtcam.6652
OAI hal-02893967v2

History
Received Jul 20, 2020
Accepted Apr 20 2021
Published Oct 5, 2021

Associate Editor
Olivier Thomas

Reviewers
Anonymous
Anonymous
Anonymous

Open Review
OAI hal-03364391

Supplementary Material
Data permalink
DOI 10.5281/zenodo.3933920

Passive discrete lens for broadband elastic guided wave focusing

Emeline Sadoulet-Reboul[1], Gaël Matten[1], Kaijun Yi[2], and Morvan Ouisse[1]

[1] Université Bourgogne Franche-Comté - FEMTO-ST Institute, Department of Applied Mechanics, 24 rue de l'Epitaphe, 25000 Besancon, France
[2] School of Aerospace Engineering, Beijing Institute of Technology, Beijing 100081, PR China

Elastic guided wave focusing is of great interest for applications such as vibroacoustic control, energy harvesting, or Structural Health Monitoring. Different strategies allow generation of this effect, GRadient-INdex devices in particular exploit medium with varying properties such as thickness to reproduce an adequate refractive index profile as in optics. The resulting continuous profiles have a curved geometry that can be hard to manufacture, and be difficult to integrate in a given design. The purpose of this paper is to propose a discrete design for a GRIN lens. It is composed of segments selected in number and thickness to give similar focusing effects as a continuous lens profile. The identified configuration is manufactured and bonded on an aluminum plate to evaluate the effective focusing performances. Numerical and experimental vibrometry results confirm that the proposed lens exhibits a fixed focal point over a broad frequency range. The discrete design overcomes fabrication issues encountered in continuous design, allowing for an easier integration in devices for elastic wave control.

Keywords: GRIN Lens, wave control, elastic waves, refractive index

1 Introduction

Focusing of elastic waves is of high interest for applications such as energy harvesting (Carrara et al. 2012; Tol et al. 2016; Hyun et al. 2019), Structural Health Monitoring (Kudela et al. 2018), or acoustic imaging (Davis et al. 2007; Deng et al. 2009; Peng et al. 2010). Indeed, by concentrating the propagating waves at an identified focal point it is possible to extract more energy, to enhance the efficiency of harvesters, to aliment small wearable autonomous devices, to spatially localize wave information, or again to increase imaging resolution and accuracy. Different strategies have emerged to achieve wave control such as Phononic Crystals (PC) consisting in periodic structures exhibiting phononic bandgaps (Timorian et al. 2020), Elastic MetaMaterials (EMMs) that exploit local resonances (Campana et al. 2020), acoustic mirrors based on specific parabolic or elliptic shapes to generate curved trajectories and localize elastic waves (Carrara et al. 2012), or continuous profile (Krylov and Tilman 2004). All these solutions can be used to give rise to GRadient-INdex devices (GRIN): their purpose is to reproduce the inhomogeneous behavior of materials in which propagating waves follow curved trajectories under adequate refractive properties as observed in optics (Gomez-Reino et al. 2002). The focus of elastic waves is realized by controlling the variations of the index of refraction or wave velocity along the axis transverse to the direction of propagation.

Gradient-Index Phononic Crystals consist of scatterers, typically inclusions as air holes or metallic inclusions, placed in an elastic matrix (silicone for instance). The acoustic velocity gradient adequate to generate the refractive index is obtained by changing the holes or inclusions radii (Sukhovich et al. 2008; Wu et al. 2011; Zhao et al. 2012), the lattice spacing (Centeno and Cassagne 2005; Kurt et al. 2008; Peng et al. 2010), or changing the elastic properties of the inclusions (Lin et al. 2009). Elastic Metamaterials (EMMs) exploit local resonances in periodic structures instead of multiple scattering, the GRIN-lens consists, in this case, of a set of solid

cylinders or pillars (Yan et al. 2013): the phase velocity is modified by spatially changing the elastic properties like the mass density profile, or similarly the thicknesses, the material or geometrical properties. By this way it is possible to create a graded impedance adapted for instance to damp travelling waves (Vemula et al. 1996). Advances in additive manufacturing techniques give emergence of 3D-printed ABH-featured beams (Chong et al. 2017) or Gradient-Index Lenses (Tol et al. 2019). While PC or EMM-based flat lenses exhibit negative refraction properties within quite narrow frequency band due to the principle linked to the dispersion bands of the structures, GRIN-based configurations allow to focus waves on larger bandwidths (Lin et al. 2009). Recent studies have shown that two-dimensional periodic lattices of Acoustic Black Holes (ABH) allow a focusing effect to be achieved on a broadband frequency band that spans the metamaterial and the phononic range (Chong et al. 2017; Zhu and Semperlotti 2017). Another strategy to focus waves consists in using acoustic mirrors with elliptical or parabolic geometries: the first developments did consist of stub extensions (Carrara et al. 2012; Carrara et al. 2013; Carrara et al. 2015) and it has been shown more recently that it was possible to improve the mirror efficiency defining a geometry-wavelength design criterion, and that the harvested power could be drastically increased using a structurally embedded mirror based on metallic spheres inserted into blind holes (Tol et al. 2017). The refractive index can also be controlled using continuously varying profiles, and changing typically the thickness or similarly the rigidity of the main structure (Krylov and Tilman 2004; Georgiev et al. 2011; Climente et al. 2014; Zareei et al. 2018): such approaches exploit the thickness-dependence of the dispersion relation of flexural waves to create an adequate gradient index. Besides, by coupling the strategies as varying simultaneously the filling fraction of a Phononic Crystal Lens and the thickness of the plate it seems possible to control not only the lowest-order antisymmetric Lamb Mode (A_0) in a plate as classically done, but to consider broadband multimodal control focusing on the two lower order Lamb Modes (A_0 and S_0) (Jin et al. 2015). Finally, semi-active, active or adaptive strategies utilize multiphysic coupling such as electromechanical or thermomechanical to control wave propagation (Yi et al. 2019; Billon et al. 2019), and have allow to develop lenses for wave focusing (Chiou et al. 2014; Yi et al. 2016; Xu et al. 2017).

Despite the development of innovative and more effective manufacturing techniques, most of the solutions presented previously are difficult to fabricate. Active solutions require to control complex and potentially sensitive multiphysical couplings. Passive solutions require precision at small scales for many unit cells, or the required curved shape for continuous profile are complex for conventional machining centres and generate a lot of manufacturing issues. The purpose of this paper is to propose a design for a passive discrete lens simpler to manufacture and that allows good focusing effect on a large frequency band. The discrete configuration is obtained from a preliminary study done on a continuous curved profile and consists in the discretization of the continuous profile into a limited number of segments. Numerical simulations and experimental results converge to show that only few segments are necessary to guide and focus waves effectively in a specific area. The passive discrete lens allows more flexibility in terms of fabrication, and does not require complex manufacturing tools. The paper is organized as follows. the design of a passive lens based on a continuous curved profile is presented in Section 2. This profile is used as a reference to propose a discrete configuration as investigated in Section 3. The obtained GRIN lens is manufactured and experimental results obtained through vibrometry measurements are compared to numerical simulations to validate the proposed design and confirm the focusing performances in Section 4. Finally, some comments and perspectives are given in the concluding section.

2 Design of a passive GRadient-Index lens based on a continuous curved profile

A GRadient-INdex lens is a structure having a profile gradient so as to reproduce the refractive index of a material. An index of refraction with an hyperbolic secant variation in the direction perpendicular to the waves' propagation direction is known to be capable of focusing waves without aberration (Lin et al. 2009). Let us consider a rectangular plate with principal direction x and in-plane perpendicular direction y, see Figure 1. The refractive index is written as $n(y) =$

$n_0 \operatorname{sech}(\alpha(y-\beta))$ where n_0 is the refractive index at lens' core ($x-$axis, $y=\beta$) and α is the gradient coefficient, see Figure 2, related to the focal length f_ℓ through $f_\ell = \pi/(2\alpha)$.

Figure 1 Plate orientation axes.

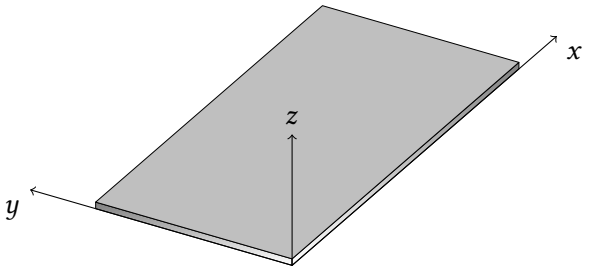

Figure 2 Refractive index defined as a hyperbolic secant function with n_0 at lens' core, and β at the focal point.

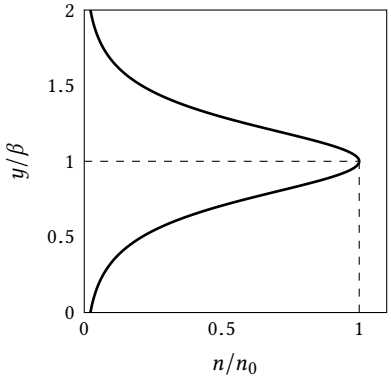

For the reference case detailed in this section, the gradient is obtained by varying the thickness of a thin plate where elastic wave focusing is expected (Zareei et al. 2018). The propagation of flexural waves in a thin plate modelled as a Kirchhoff–Love plate is described by a fourth-order partial differential equation

$$D\nabla^4 w + \rho h \frac{\partial^2 w}{\partial t^2} = 0 \tag{1}$$

where w is the transverse displacement of the plate, $D = Eh^3/(12\rho(1-\nu^2))$, the flexural rigidity of the plate, E, the Young's modulus, ν, Poisson's ratio, ρ, the density and h, the thickness of the plate. For a harmonic wave propagation, the dispersion relationship that links the wavenumber k to the angular frequency ω for flexural waves can be written as $Dk^4 = \rho h \omega^2$. The wave propagation is considered in the main direction x of the plate and the thickness is assumed to vary only in the y-direction, and is thus constant along x. Finally, the phase velocity c satisfies

$$c^4 = \frac{k^4}{\omega^4} = \frac{Eh^2\omega^2}{12\rho(1-\nu^2)}. \tag{2}$$

Referring to optics, the refractive index n is defined as the ratio of the velocity c_0 of the waves in the homogeneous plate with initial fixed thickness h_0 to their velocity c in the lens with varying thickness h, that is $n(y) = c_0/c(y)$. If the lens material is the same as the plate material and does not depend on space, the gradient of the refractive index is directly linked to the gradient of the thickness $n(y) = \sqrt{h_0/h(y)}$ with

$$h(y) = \frac{h_0}{n_0^2}\cosh^2[\alpha(y-\beta)]. \tag{3}$$

Since this relation does not depend on the angular frequency, it is valid for any excitation frequency and thus a focusing effect on a wide frequency band can be expected.

In the remainder of the document, all illustrated velocity fields have the same scale and colormap indicated in Figure 3.

Figure 3 Velocity field scale and colormap.

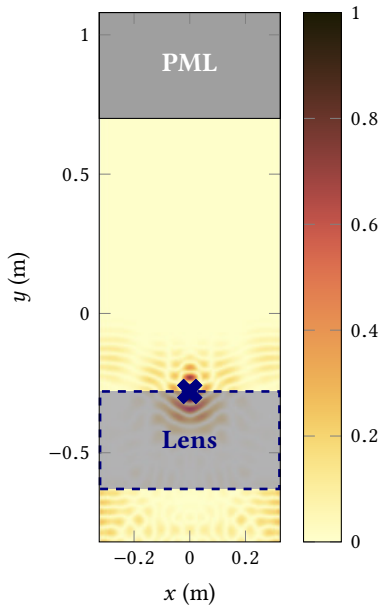

2.1 Case of a symmetrical GRIN lens

For the first application case the GRIN lens is designed to be symmetrical with respect to the mid-plane of the thin plate considering the symmetry of the propagating medium: Figure 4 shows the evolution of the thickness of the lens to generate the refractive profile proposed in Equation (3). The host plate is 5 mm thick, 1.9 m long, and 0.65 m wide. It is made of aluminum with properties $E = 70$ Gpa for the Young's modulus, $\nu = 0.3$ for the Poisson's ratio, $\rho = 2700\,\mathrm{kg/m^3}$ for the density. The lens consists in an aluminum plate with the same properties as the host plate. It is 0.65 m wide as the host plate, and 0.35 m long. The gradient coefficient α is chosen for the focal length to be equal to 0.35 cm, meaning that the focal point should be at the exit of the lens. The thickness of the lens follows the profile defined by Equation (3). It is bonded to the plate with an assumption of perfect continuity of displacements between the two structures. All the parameters for the studies are recalled in appendix A. The FE method is used to simulate the

Figure 4 Profile of the symmetrical GRIN lens.

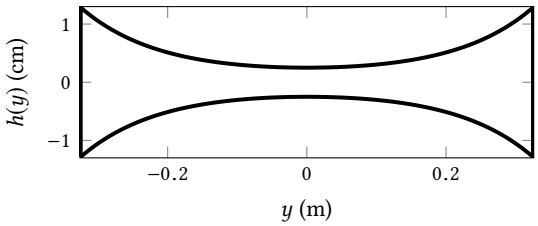

wave propagation in a plate incorporating the symmetrical GRIN lens. In order to excite the structure, a plane wave front is generated by an array of 18 piezoelectric transducers (PIC 151, 3 cm × 3 cm × 0.5 mm) bonded to the aluminum plate with equal spacing (around 6.5 mm). A Perfectly Matched Layer (PML) is introduced at the boundary of the plate to absorb outgoing waves, simulating an infinite plate and minimizing reflections. Numerical simulations are done using the commercial software Comsol Multiphysics® (COMSOL 2021). Figure 5 presents the full problem studied as well as the Finite Element mesh used for the study. It is composed of quadratic brick elements that were necessary for the electromechanical simulation despite the thin thicknesses involved. The maximum element length is chosen to ensure eight mesh elements per wavelength, and a distribution of two elements in the thickness is imposed. A multiphysics frequency domain simulation is performed in order to solve simultaneously the electrostatics and the solid mechanics equations for the frequencies $f = 2350$ Hz, 3450 Hz, 4400 Hz, 5300 Hz, 6850 Hz and 7900 Hz. The normalized transverse velocity fields obtained are presented in Figure 6. Normalization is based on the maximum value of the field. It can be observed that, as expected, waves join the focal point indicated by a dark blue cross, and then propagate in the main direction of the plate.

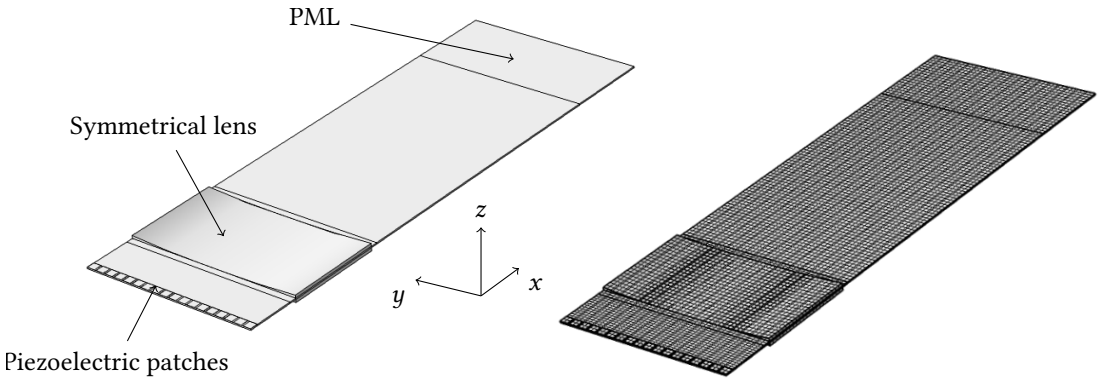

Figure 5 Integration of the symmetrical GRIN lens in the plate to focus elastic transversal waves. [Left] Piezoelectric patches used to generate an incident plane wave front: a Perfectly Matched Layer (PML) introduced at the boundary to avoid reflections. [Right] Corresponding finite element mesh.

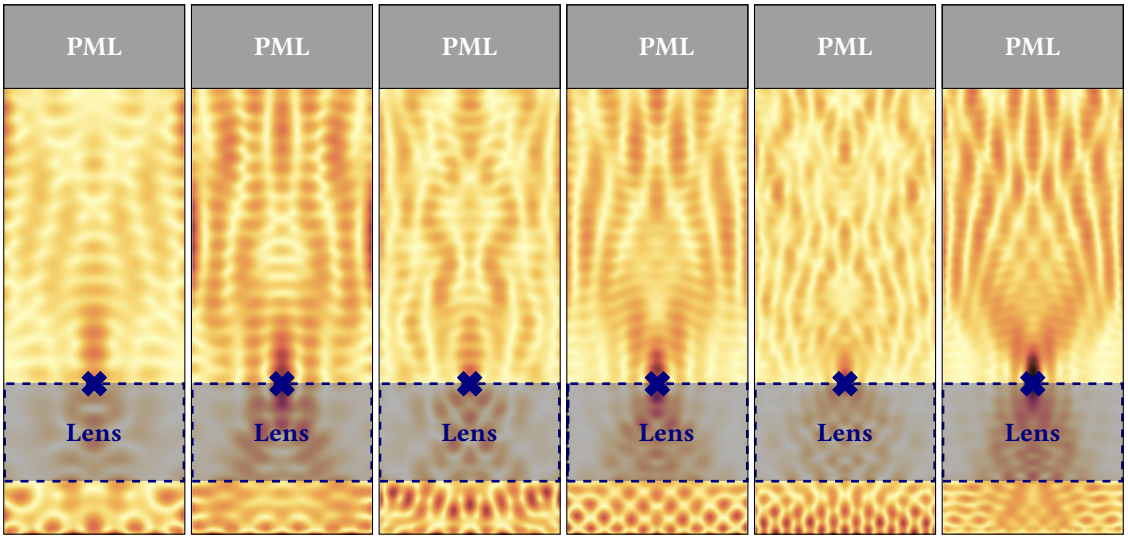

(a) $f = 2350$ Hz **(b)** $f = 3450$ Hz **(c)** $f = 4400$ Hz **(d)** $f = 5300$ Hz **(e)** $f = 6850$ Hz **(f)** $f = 7900$ Hz

Figure 6 Nondimensional transverse velocity amplitude for various excitation frequencies f computed with a symmetrical continuous lens.

It can be observed from numerical simulations that the focusing effect is always visible at the expected focal point for all the frequencies.

2.2 Case of a unsymmetrical GRIN lens

One major difficulty with the symmetrical GRIN lens is the needed space as both sides of the plate are covered. For this reason a second application is considered to investigate the focus efficiency that can be obtained with an unsymmetrical GRIN lens. The new profile is presented in Figure 7. Same simulations as for the symmetrical lens are completed and the results obtained for

Figure 7 Profile of the unsymmetrical GRIN lens.

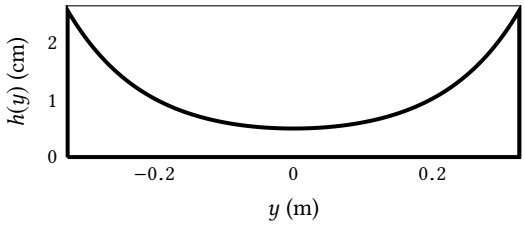

the different frequencies are presented in Figure 8. The focusing effect still appears on the whole frequency band, even if it is more pronounced for higher frequencies.

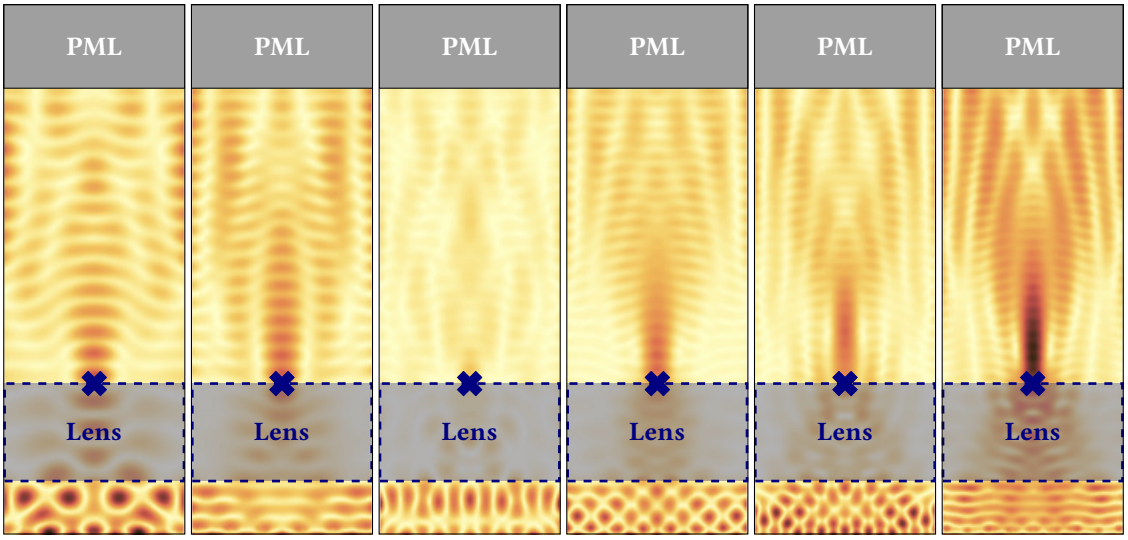

(a) $f = 2350$ Hz **(b)** $f = 3450$ Hz **(c)** $f = 4400$ Hz **(d)** $f = 5300$ Hz **(e)** $f = 6850$ Hz **(f)** $f = 7900$ Hz

Figure 8 Normalized transverse velocity amplitude for various excitation frequencies computed with a unsymmetrical continuous lens.

3 Design of a passive GRadient-Index lens based on a discrete curved profile

The previous section has shown that it is possible to obtain good focusing effects on a large frequency band using an unsymmetrical GRadient-Index lens. Despite the unilateral design, the continuous curved profile remains difficult to manufacture which can be an obstacle for industrial applications. For this reason it is proposed to study the possibility to obtain similar focusing effects as for the continuous case using a discrete curved profile. Thus, the unsymmetrical profile is divided into segments, and three configurations are considered, arbitrary fixed to 7, 11 and 15 segments. All segments have the same width and their thicknesses correspond to the average of the thickness values given by the continuous profile at the ends of each segment. It is possible to use optimisation methods to identify a one-sided discrete distribution that achieves focusing effects similar to the symmetric configuration. Such an approach has not been adopted here as an objective was to define a design easy to manufacture: in this context, a strategy with so few segments of the same size has been retained. Figure 9 presents the associated discrete profiles for the lens.

Figure 9 Discretization of the continuous GRIN-lens profile into (a) 7 segments, (b) 11 segments, and (c) 15 segments.

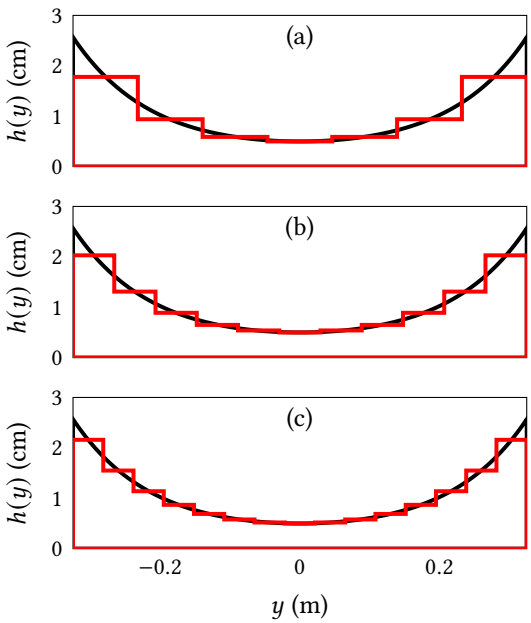

3.1 Discretization of the curved profile

To estimate an adequate discretization of the curved profile, numerical simulations are performed to compare the amplitude of the quadratic transverse velocity of the plate obtained along the central line in the direction of the plate that crosses the focal point. The symmetrical continuous profile is always used as a reference as this configuration corresponds to the optimal case. Figure 10 presents the obtained results: they are normalized to the maximum value to be comparable. The vertical dot lines indicate the position of the GRIN lens.

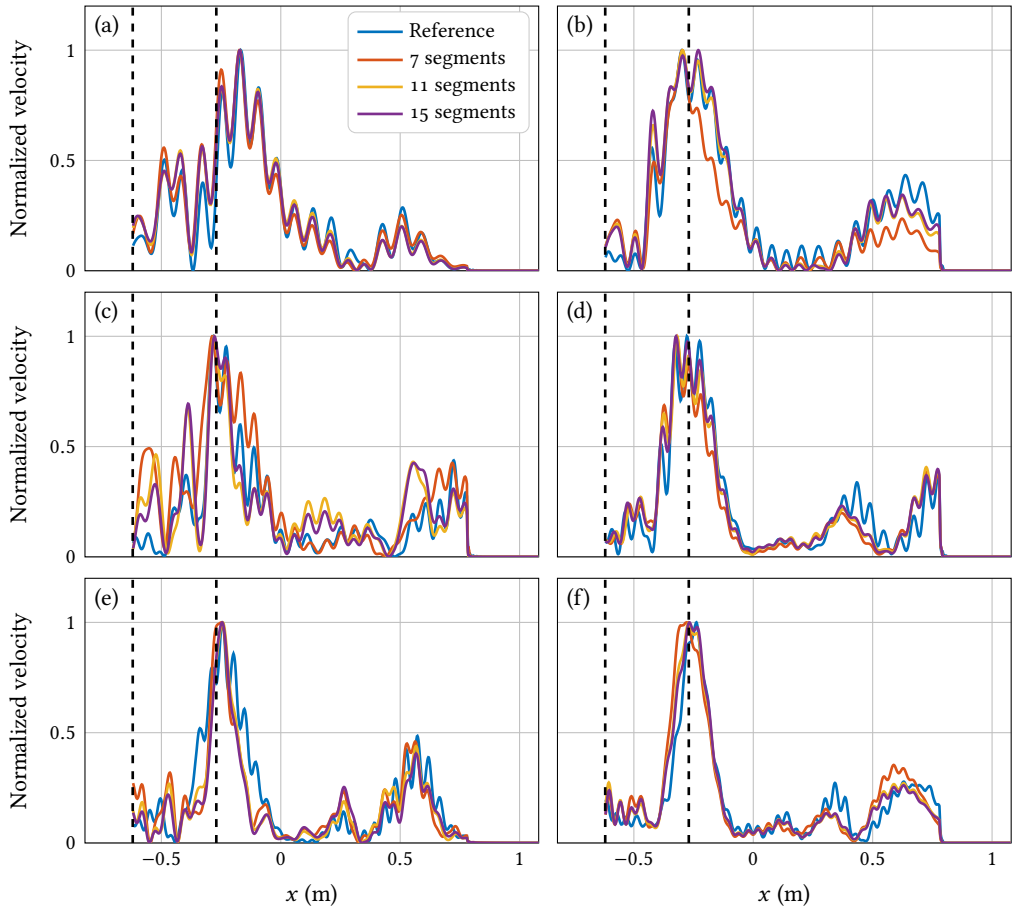

Figure 10 Normalized quadratic transverse velocity along the central line in the direction of the plate for various frequencies from (a) 2350 Hz to (f) 7900 Hz—see Figure 8.

The purpose is to verify whether point focus properties similar to those obtained with the symmetrical continuous lens can be obtained with a one-sided discrete lens. It can be observed that all curves present a similar overall behavior, and for information purposes, the L^2 relative error norm on the normalized amplitude of the quadratic transverse velocity around the estimated focal point is given in Table 1. Globally, the results converge to the reference ones as the number of segments increases, and it appears that only seven segments are enough to obtain good focusing effects.

Table 1 L^2 relative error norm (in %) on the normalized amplitude of the quadratic transverse velocity around the estimated focal point.

Frequency	7 segments	11 segments	15 segments
2350	7.2	6.1	6.1
3450	1.6	2.3	2.9
4400	9.2	8.2	10.6
5300	13	8.9	2.8
6850	11.3	8.2	8.3
7900	9.4	3	3

The higher the frequency, the stronger the focusing effect and the more centred in a point it is. Following these conclusions, the proposed unsymmetrical discrete lens is composed of seven segments with identical widths equal to 92.8 mm and respective thicknesses given in Table 2.

Table 2 Heights of the seven segments composing the lens from the left edge to the right edge.

Segment	Height [mm]
Segment 1	12.8
Segment 2	4.4
Segment 3	1.9
Segment 4	0.0
Segment 5	1.9
Segment 6	4.4
Segment 7	12.8

4 Validation of the discrete GRIN lens by comparison of experimental and numerical results

In order to perform experiments, the elements composing the lens are manufactured using electroerosion cutting. Due to the symmetry of the lens, two series of three elements with different thicknesses are manufactured, no element is introduced in the center of the lens. They are bonded on a host plate. Figure 11(a) presents the experimental set-up with the aluminum plate mounted on a frame for laser vibrometry measurements, and Figure 11(b), the bonded GRIN lens. The set of 18 piezoelectric transducers used to generate propagating plane waves is visible at the lower edge of the plate. At the top edge a viscoelastic constrained layer is introduced in order to reproduce PML effects, absorb incoming waves and avoid reflections. The layer is made with a 3M VHB polymer, it is 30 cm wide and 3 mm thick. It is constrained thanks to a 1 mm thick aluminum plate: the optimal thickness to ensure the best absorption has been obtained from preliminary numerical simulations.

Figure 11 Experimental setup: (a) Nude plate suspended to a frame with piezoelectric patches at the lower edge and a constrained viscoelastic layer at the top edge; (b) View of the discrete GRIN lens bonded on the plate.

Wavelets at central frequencies are applied to the transducers using a numerical circuit and a voltage amplifier. The transverse velocity of the plate is measured in the time domain on a grid of points using a Polytec infrared scanning laser vibrometer (PSV 500 X-tra). As previously, the FE method is used to compute the transverse velocity for the case of the GRIN discrete lens. The same set of piezoelectric patches is used to generate a plane wave front, and a PML layer is introduced to prevent reflections. Experimental and numerical studies are here done in the time domain. Field representations are solutions obtained at specific times corresponding to focusing at the expected focal point.

Figures 12 to 17 present snapshots of the amplitudes of the experimental and numerical normalized transverse velocities as well as a comparison between the quadratic velocities on the

central line in the direction of wave propagation, for frequencies 2350 Hz (case 1), 3450 Hz (case 2), 4400 Hz (case 3), 5300 Hz (case 4), 6850 Hz (case 5), and 7900 Hz (case 6). The domain chosen for the comparison between results is set behind the lens. Numerical and experimental results are in good agreement: they confirm the existence of a similar focal point for all the studied frequencies where the wave energy concentrates. The focusing effect is all the more visible and pronounced that frequencies are high, but it is noticeable that the effect is visible for all the studied frequencies.

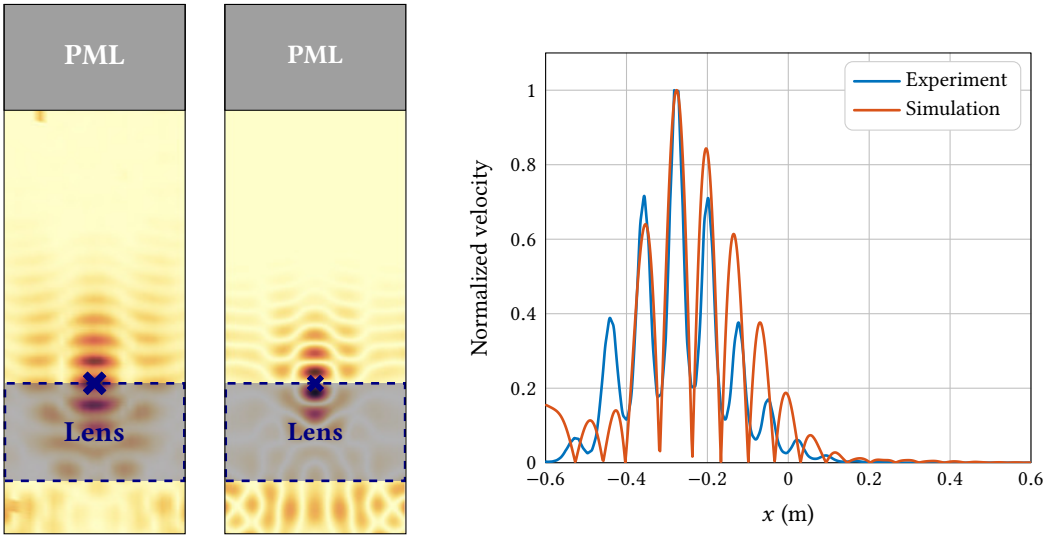

(a) Experiment **(b)** Simulation **(c)** Comparison

Figure 12 Normalized transverse velocity amplitude for a GRIN discrete lens for $f = 2350$ Hz.

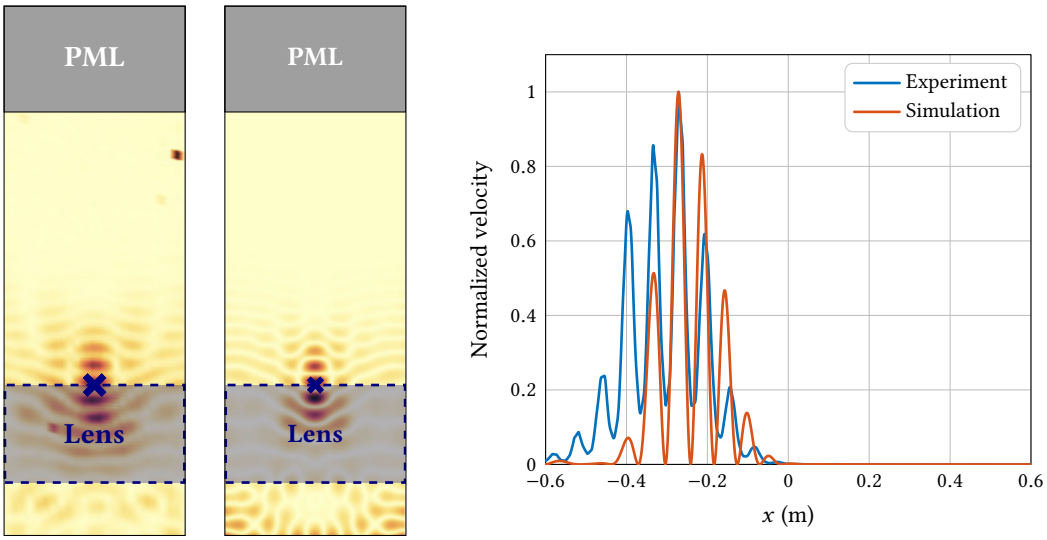

(a) Experiment **(b)** Simulation **(c)** Comparison

Figure 13 Normalized transverse velocity amplitude for a GRIN discrete lens for $f = 3450$ Hz.

5 Conclusion

The paper proposes a design for a passive discrete GRIN lens to focus elastic waves. The discrete configuration consists in a set of segments with varying thicknesses in order to generate a refractive index for wave focusing. Numerical simulations done on different discrete configurations and compared to a continuous reference profile show that a reduced number of segments is enough to obtain good focusing effects. The designed GRIN lens has been manufactured and vibrometry measurements done to measure the transverse velocity on a plate equipped with the lens for different frequencies confirm the existence of a similar focal point where wave energy is

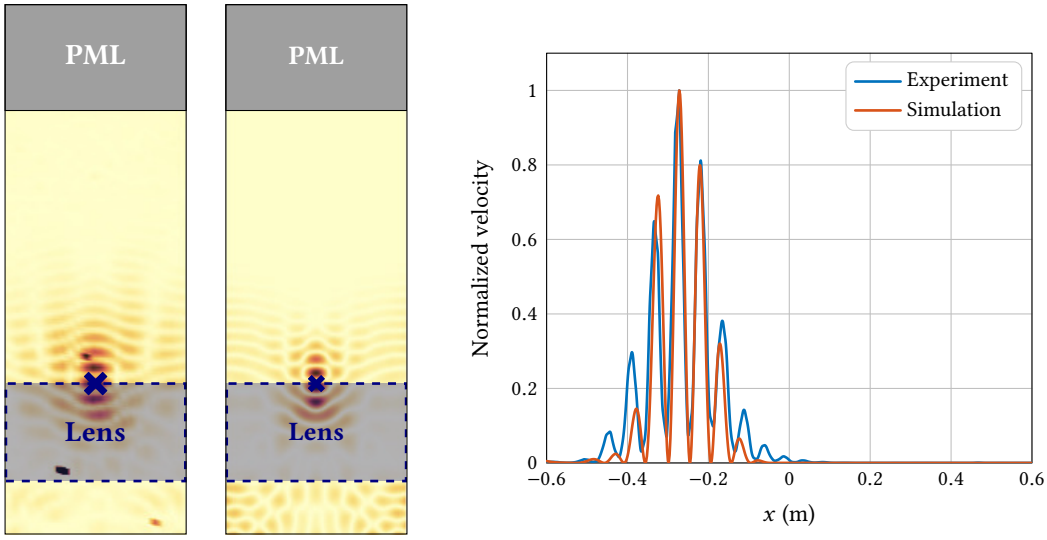

(a) Experiment **(b)** Simulation **(c)** Comparison

Figure 14 Normalized transverse velocity amplitude for a GRIN discrete lens for $f = 4400$ Hz.

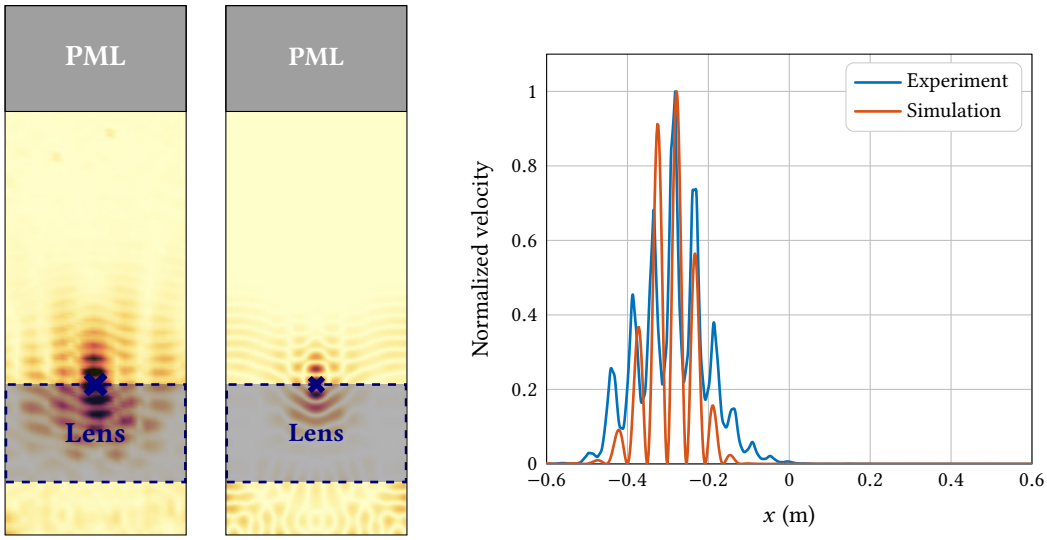

(a) Experiment **(b)** Simulation **(c)** Comparison

Figure 15 Normalized transverse velocity amplitude for a GRIN discrete lens for $f = 5300$ Hz.

concentrated. The proposed design is interesting as focusing effects resulting in a concentration of elastic waves at one point of the structure are obtained on a wide range of frequencies, and the very simplified configuration based on the bonding of segments significantly reduces the fabrication complexity compared to continuous profiles. This paves the way for simpler focusing device integration strategies for vibroacoustic control or energy harvesting for instance.

References

Billon, K, M Ouisse, E Sadoulet-Reboul, M Collet, P Butaud, G Chevallier, and A Khelif (2019). Design and experimental validation of a temperature-driven adaptive phononic crystal slab. *Smart Materials and Structures* 28(3):035007. [DOI], [HAL].

Campana, M., M. Ouisse, E. Sadoulet-Reboul, M. Ruzzene, S. Neild, and F. Scarpa (2020). Impact of non-linear resonators in periodic structures using a perturbation approach. *Mechanical Systems and Signal Processing* 135:106408. [DOI], [OA].

Carrara, M., M. R. Cacan, M. J. Leamy, M. Ruzzene, and A. Erturk (2012). Dramatic enhancement of structure-borne wave energy harvesting using an elliptical acoustic mirror. *Applied Physics Letters* 100(20):204105. [DOI].

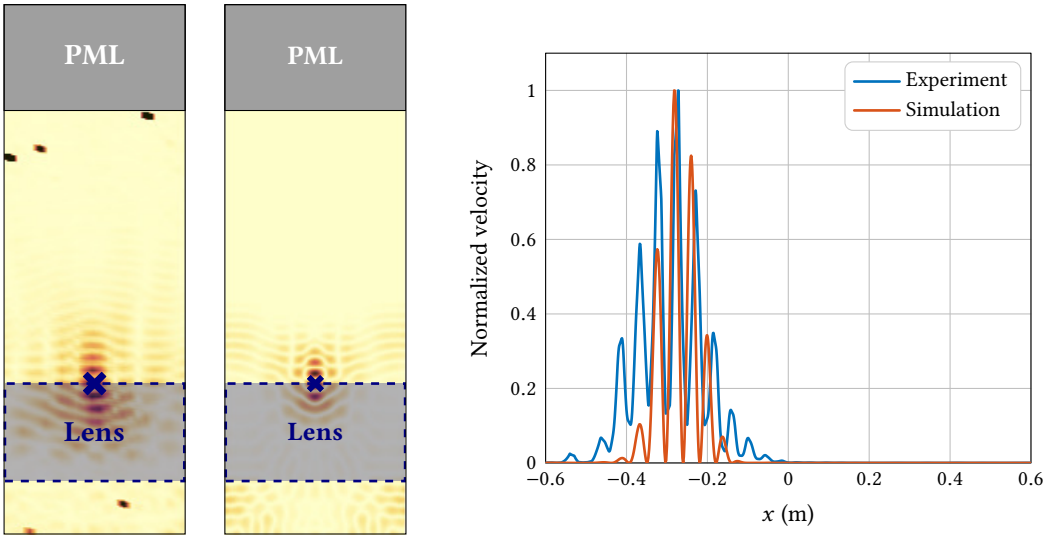

(a) Experiment **(b)** Simulation **(c)** Comparison

Figure 16 Normalized transverse velocity amplitude for a GRIN discrete lens for $f = 6850$ Hz.

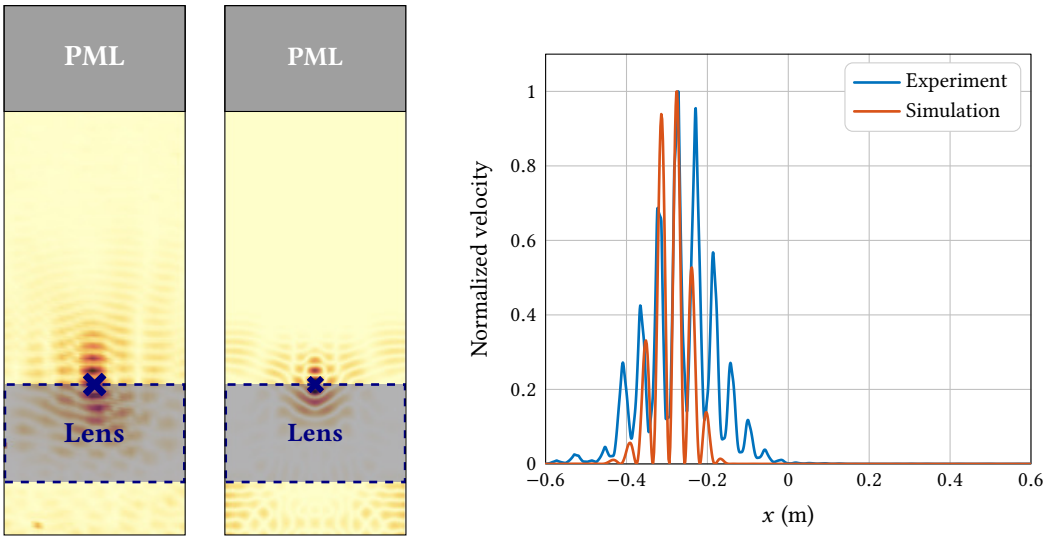

(a) Experiment **(b)** Simulation **(c)** Comparison

Figure 17 Normalized transverse velocity amplitude for a GRIN discrete lens for $f = 7900$ Hz.

Carrara, M, M. R. Cacan, J Toussaint, M. J. Leamy, M Ruzzene, and A Erturk (2013). Metamaterial-inspired structures and concepts for elastoacoustic wave energy harvesting. *Smart Materials and Structures* 22(6):065004. [DOI].

Carrara, M., J. A. Kulpe, S. Leadenham, M. J. Leamy, and A. Erturk (2015). Fourier transform-based design of a patterned piezoelectric energy harvester integrated with an elastoacoustic mirror. *Applied Physics Letters* 106(1):013907. [DOI].

Centeno, E. and D. Cassagne (2005). Graded photonic crystals. *Optics Letters* 30(17):2278. [DOI].

Chiou, M.-J., Y.-C. Lin, T. Ono, M. Esashi, S.-L. Yeh, and T.-T. Wu (2014). Focusing and waveguiding of Lamb waves in micro-fabricated piezoelectric phononic plates. *Ultrasonics* 54(7):1984–1990. [DOI].

Chong, B. M. P., L. B. Tan, K. M. Lim, and H. P. Lee (2017). A review on acoustic black-holes (ABH) and the experimental and numerical study of ABH-featured 3D printed beams. *International Journal of Applied Mechanics* 09(06):1750078. [DOI].

Climente, A., D. Torrent, and J. Sánchez-Dehesa (2014). Gradient index lenses for flexural waves based on thickness variations. *Applied Physics Letters* 105(6):064101. [DOI], [OA].

COMSOL (2021). *COMSOL Multiphysics®*. Version 5.6.

Davis, M., R. Greegor, K. Li, J. Nielsen, C. Parazzoli, and M. Tanielian (2007). *Metamaterial scanning lens antenna systems and methods*. US Patent 7,218,285.

Deng, K., Y. Ding, Z. He, H. Zhao, J. Shi, and Z. Liu (2009). Graded negative index lens with designable focal length by phononic crystal. *Journal of Physics D: Applied Physics* 42(18):185505. [DOI].

Georgiev, V., J. Cuenca, F. Gautier, L. Simon, and V. Krylov (2011). Damping of structural vibrations in beams and elliptical plates using the acoustic black hole effect. *Journal of Sound and Vibration* 330(11):2497–2508. [DOI].

Gomez-Reino, C., M. V. Perez, and C. Bao (2002). *Gradient-index optics. fundamentals and applications*. Springer Berlin Heidelberg. [DOI].

Hyun, J., W. Choi, and M. Kim (2019). Gradient-index phononic crystals for highly dense flexural energy harvesting. *Applied Physics Letters* 115(17):173901. [DOI].

Jin, Y., D. Torrent, Y. Pennec, Y. Pan, and B. Djafari-Rouhani (2015). Simultaneous control of the So and Ao Lamb modes by graded phononic crystal plates. *Journal of Applied Physics* 117(24):244904. [DOI].

Krylov, V. and F. Tilman (2004). Acoustic 'black holes' for flexural waves as effective vibration dampers. *Journal of Sound and Vibration* 274(3-5):605–619. [DOI].

Kudela, P., M. Radzienski, W. Ostachowicz, and Z. Yang (2018). Structural Health Monitoring system based on a concept of Lamb wave focusing by the piezoelectric array. *Mechanical Systems and Signal Processing* 108:21–32. [DOI], [OA].

Kurt, H., E. Colak, O. Cakmak, H. Caglayan, and E. Ozbay (2008). The focusing effect of graded index photonic crystals. *Applied Physics Letters* 93(17):171108. [DOI], [OA].

Lin, S.-C. S., T. J. Huang, J.-H. Sun, and T.-T. Wu (2009). Gradient-index phononic crystals. *Physical Review B* 79(9):094302. [DOI].

Peng, S., Z. He, H. Jia, A. Zhang, C. Qiu, M. Ke, and Z. Liu (2010). Acoustic far-field focusing effect for two-dimensional graded negative refractive-index sonic crystals. *Applied Physics Letters* 96(26):263502. [DOI].

Sukhovich, A., L. Jing, and J. H. Page (2008). Negative refraction and focusing of ultrasound in two-dimensional phononic crystals. *Physical Review B* 77(1):014301. [DOI].

Timorian, S., M. Ouisse, N. Bouhaddi, S. De Rosa, and F. Franco (2020). Numerical investigations and experimental measurements on the structural dynamic behaviour of quasi-periodic meta-materials. *Mechanical Systems and Signal Processing* 136:106516. [DOI], [HAL].

Tol, S., F. L. Degertekin, and A. Erturk (2016). Gradient-index phononic crystal lens-based enhancement of elastic wave energy harvesting. *Applied Physics Letters* 109(6):063902. [DOI].

Tol, S., F. L. Degertekin, and A. Erturk (2017). Structurally embedded reflectors and mirrors for elastic wave focusing and energy harvesting. *Journal of Applied Physics* 122(16):164503. [DOI].

Tol, S., F. Degertekin, and A. Erturk (2019). 3D-printed phononic crystal lens for elastic wave focusing and energy harvesting. *Additive Manufacturing* 29:100780. [DOI], [OA].

Vemula, C., A. Norris, and G. Cody (1996). Attenuation of waves in plates and bars using a graded impedance interface at edges. *Journal of Sound and Vibration* 196(1):107–127. ISSN: 0022-460X. [DOI].

Wu, T.-T., Y.-T. Chen, J.-H. Sun, S.-C. S. Lin, and T. J. Huang (2011). Focusing of the lowest antisymmetric Lamb wave in a gradient-index phononic crystal plate. *Applied Physics Letters* 98(17):171911. [DOI].

Xu, J., S. Li, and J. Tang (2017). Adaptive GRIN lens based on piezoelectric metamaterial for acoustic beam focusing. *Active and Passive Smart Structures and Integrated Systems 2017*. Vol. 10164. International Society for Optics and Photonics. SPIE, 101641S. [DOI].

Yan, X., R. Zhu, G. L. Huang, and F. G. Yuan (2013). Focusing flexural Lamb waves by designing elastic metamaterials bonded on a plate. *Health Monitoring of Structural and Biological Systems 2013*. Vol. 8695. International Society for Optics and Photonics. SPIE, 86952P. [DOI].

Yi, K, M Collet, M Ichchou, and L Li (2016). Flexural waves focusing through shunted piezoelectric patches. *Smart Materials and Structures* 25(7):075007. [DOI], [HAL].

Yi, K., M. Ouisse, E. Sadoulet-Reboul, and G. Matten (2019). Active metamaterials with broadband controllable stiffness for tunable band gaps and non-reciprocal wave propagation. *Smart Materials and Structures* 28(6):065025. [DOI], [HAL].

Zareei, A., A. Darabi, M. J. Leamy, and M.-R. Alam (2018). Continuous profile flexural GRIN lens: Focusing and harvesting flexural waves. *Applied Physics Letters* 112(2):023901. [DOI].

Zhao, J., R. Marchal, B. Bonello, and O. Boyko (2012). Efficient focalization of antisymmetric Lamb waves in gradient-index phononic crystal plates. *Applied Physics Letters* 101(26):261905. [DOI].

Zhu, H. and F. Semperlotti (2017). Two-dimensional structure-embedded acoustic lenses based on periodic acoustic black holes. *Journal of Applied Physics* 122(6):065104. [DOI], [ARXIV].

A Parameters

Table A.1 contains all the geometrical and material parameters used for the numerical simulations.

Parameter	Variable [Unit]	Value
Plate		
L	Length [m]	1.9
w	width [m]	0.065
h_0	thickness [m]	0.005
E	Young's modulus [GPa]	70
ρ	density [kg m^{-3}]	2700
ν	Poisson's ratio	0.3
Piezoelectric patches		
l_p	length [m]	0.03
w_p	width [m]	0.03
h_p	thickness [m]	0.005
ρ_p	density [kg m^{-3}]	7760
$\epsilon_1^\sigma = \epsilon_2^\sigma$, ϵ_3^σ	dielectric permittivity	1936 ϵ_0, 2109 ϵ_0
Compliance matrix under constant electric field		
$S_{11}^E = S_{22}^E$, S_{33}^E	[Pa^{-1}]	1.683×10^{-11}, 1.9×10^{-11}
S_{12}^E, $S_{13}^E = S_{23}^E$	[Pa^{-1}]	-5.656×10^{-12}, -7.707×10^{-12}
$S_{44}^E = S_{55}^E$, S_{66}^E	[Pa^{-1}]	5.096×10^{-11}, 4.497×10^{-11}
Piezoelectric matrix		
$d_{31} = d_{32}$	[C/N]	-2.14×10^{-10}
d_{33}	[C/N]	4.23×10^{-10}
$d_{24} = d_{15}$	[C/N]	6.1×10^{-10}
PML		
ℓ_pml	length [m]	0.3
w_pml	width [m]	$0.65 = w$
h_pml	thickness [m]	$0.005 = w$

Table A.1 Parameters for the numerical simulations.

Authors' contributions All the authors conceived the presented ideas. K.Y. and E.SR. performed the numerical computations. G.M. carried out the experiments. E.SR. and M.O. performed the post-treatment. E.SR. wrote the initial draft and all the authors discussed the results and proposed corrections.

Supplementary Material Videos presenting the wave propagation obtained numerically and experimentally in the plate with the GRIN lens composed of seven segments are available as supplementary material at the permalink 10.5281/zenodo.3933920. Three frequencies are considered (2350 Hz, 5300 Hz and 7900 Hz), and these results correspond to those in Figure 12, Figure 15 and Figure 17.

Acknowledgements This work has been supported by the EUR EIPHI Project (contract ANR-17-EURE-0002) and Bourgogne Franche-Comté Region. Authors want to thank the C.F.A.I from Besançon and in particular Simon Huot for their precious help in the manufacture of the lens elements.

Ethics approval and consent to participate Not applicable

Consent for publication Not applicable

Competing interests The authors declare that they have no competing interests.

Journal's Note JTCAM remains neutral with regard to the content of the publication and institutional affiliations.